Comparative analysis of robust entanglement generation in engineered XX spin chains

Eduardo K. Soares, G. D. de Moraes Neto and Fabiano M. Andrade

***Abstract*— We numerically compare two entanglement generation protocols in finite XX spin chains with spin magnitudes $s = 1/2, 1, 3/2$. Protocol 1 (P1) uses staggered couplings to create entanglement in its extremes, while Protocol 2 (P2) adopts a dual-port architecture with optimized boundary fields to mediate virtual excitations between terminal spins. P2 consistently outperforms P1 across all spin values, generating higher-fidelity entanglement in shorter times. It also shows greater robustness under realistic imperfections. The scalability, efficiency, and noise resilience of P2 make it a strong candidate for entanglement distribution in solid-state quantum technologies.**

***Keywords*— quantum spin chains, entanglement generation, XX model, quantum information transfer.**

I. Introduction

The advancement of quantum technologies depends crucially on the ability to generate and control quantum resources in a reliable and scalable way [1], [2]. Among these resources, quantum entanglement stands out as a fundamental ingredient, enabling powerful protocols to operate within the limits of local operations and classical communication (LOCC) [2]. Entangled states are at the heart of quantum information processing tasks, such as teleportation [3], sensing [4], and communication [5]. In particular, maximally entangled states, such as Bell pairs (EPR states), are essential building blocks for these applications [6].

Scalable solid-state quantum processors require architectures that can produce and distribute entanglement on demand, integrated directly with quantum registers [7]. Spin chains have thus emerged as promising candidates for short-range quantum communication and entanglement distribution [8], due to their tunability and compatibility with solid-state platforms.

We compare two entanglement generation protocols based on XX-type spin chains: Protocol 1 (P1), where alternating weak and strong couplings guide quantum correlations toward the chain edges [9], and Protocol 2 (P2), which employs symmetric perturbative couplings at both ends to enhance transport speed and facilitate the buildup of quantum correlations [10].

Using the XX spin model, we systematically investigated the entanglement dynamics for spins $s = 1/2$, 1, and $3/2$ under both ideal and noisy conditions. Our analysis is based on extensive numerical simulations, quantifying entanglement via the negativity measure, explicitly including the effects of static disorder and local decoherence.

Eduardo K. Soares, Programa de Pós-Graduação em Ciências/Física, Universidade Estadual de Ponta Grossa, Ponta Grossa-PR, e-mail: edukso2002@gmail.com; G. D. de Moraes Neto, College of Physics and Engineering, Qufu Normal University, Qufu-China, e-mail:gdmneto@gmail.com; Fabiano M. Andrade, Departamento de Matemática e Estatística, Universidade Estadual de Ponta Grossa, Ponta Grossa-PR, e-mail: fmandrade@uepg.br. Este trabalho foi parcialmente financiado por CNPq (313124/2023-0).

Although effective Hamiltonians are derived, our conclusions rely on numerical data. Importantly, we observe that the dual-port databus protocol (P2) enables faster and more robust entanglement generation than the staggered (P1) scheme, especially in the presence of noise and imperfections. Our results are relevant to systems such as trapped ions [11], superconducting qubit arrays [12], NV centers in diamond [13], and quantum dot devices [14], where engineered spin-spin interactions and coherent control have been realized. This work thus paves the way for deterministic and scalable entanglement sources in next-generation quantum processors and networks [15].

II. Model and Methods

We model the system as an N-site XX spin chain with Hamiltonian

$$H = \sum_{i=1}^{N-1} J_i \left(S_i^x S_{i+1}^x + S_i^y S_{i+1}^y \right) + \sum_{i=1}^{N} B_i S_i^z, \qquad (1)$$

where S_i^α are spin-s operators and B_i are local magnetic fields. The coupling constants J_i alternate between two values, Δ and δ, depending on the position in the chain (see Fig. 1).

The system evolves under the Lindblad master equation

$$\dot{\rho} = -i[H, \rho] + \gamma \sum_{i=1}^{N} \left(S_i^z \rho S_i^z - \frac{1}{2} S_i^z S_i^z, \rho \right), \qquad (2)$$

where γ introduces local pure dephasing, a dominant decoherence source in many platforms [16], [17], [12], [18]. Unless otherwise stated, we set $\gamma = 0$ to focus on coherent dynamics, but also consider finite γ to assess noise resilience.

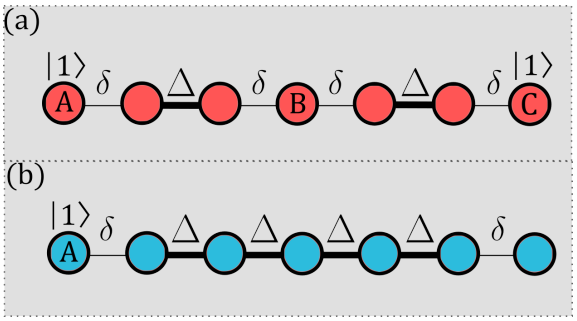

Fig. 1
(A) P1 AND (B) P2 ARCHITECTURES. BOLD LINES REPRESENT Δ COUPLINGS, WHILE THIN LINES INDICATE δ COUPLINGS.

We quantify entanglement between boundary spins using the negativity [19],

$$\mathcal{N}(\hat{\rho}) = \frac{\|\hat{\rho}^{T_A}\|_1 - 1}{2}, \tag{3}$$

and normalize it to the maximum value for the given spin s. To check if the generated state matches a Bell state, we compute fidelity

$$F(\hat{\rho}, \hat{\sigma}) = \left(\mathrm{tr}\sqrt{\sqrt{\hat{\rho}}\hat{\sigma}\sqrt{\hat{\rho}}}\right). \tag{4}$$

A. Entanglement Generation Protocols

We explore two entanglement generation protocols (Fig. 1), both designed to create quantum correlations between boundary spins.

In P1, the chain is initialized as

$$|\psi(0)\rangle = |1\rangle_A \otimes |0\rangle^{\otimes N-2} \otimes |1\rangle_C, \tag{5}$$

with $B_i = 0$. The boundary spins start excited, while the bulk is in the ground state. Entanglement arises from coherent exchanges across the chain.

In P2, the initial state is

$$|\psi(0)\rangle = |1\rangle_A \otimes |0\rangle^{\otimes N-1}, \tag{6}$$

but here, a single excitation is localized at the sender (s) site, while all other spins, including the receiver (r) at the opposite end, begin in the unexcited state. For a spin-s system, we define the computational basis states in terms of the eigenstates of the S_z operator. Specifically, for spin-1, the basis states are $|0\rangle \equiv |m = -1\rangle$, $|1\rangle \equiv |m = 0\rangle$, and $|2\rangle \equiv |m = +1\rangle$. For spin-3/2, the definitions are $|0\rangle \equiv |m = -3/2\rangle$, $|1\rangle \equiv |m = -1/2\rangle$, $|2\rangle \equiv |m = +1/2\rangle$, and $|3\rangle \equiv |m = +3/2\rangle$.

Initial state preparation follows a consistent scheme across the different spin systems. In P1, the bulk spins are initialized in the minimal S_z eigenstate, $|m = -s\rangle$, corresponding to the lowest indexed basis state $|0\rangle$, while the boundary spins are set to the maximal eigenstate, $|m = +s\rangle$, corresponding to the highest indexed basis state. In contrast, P2 initializes all spins uniformly in the minimal eigenstate $|m = -s\rangle$.

P2 keeps the bulk largely unexcited, with virtual excitations mediating indirect coupling between the ends. This minimizes exposure to disorder and noise, enhancing robustness.

While related to state-transfer schemes, the goal here is not high-fidelity transmission but efficient entanglement generation. We compare P1 and P2 across spin values $s = 1/2, 1, 3/2$, and study their performance under disorder and dephasing.

Our analysis shows P2 has key advantages: (i) faster entanglement buildup, especially for $s = 1/2$; (ii) better resilience to disorder and dephasing; (iii) stronger performance in higher-spin systems where P1 is less effective.

These benefits stem from virtual bulk excitation and boundary control, allowing coherent dynamics that bypass bulk-induced decoherence.

Other methods for long-distance entanglement include dimerized ground states [20], dissipative engineering [21], [22], measurement-based post-selection [23], and topological edge modes [24]. While we do not benchmark against these here, our protocols complement this broader landscape.

III. Results

A. Benchmark without noise: dynamics in pristine chains

To establish a baseline, we first compare the coherent dynamics of the two architectures in the absence of disorder or decoherence for $N = 7$. Figure 2 shows the time evolution of the end-to-end negativity for spin magnitudes $s = 1/2$, 1, and $3/2$. The results demonstrate that P2 reaches its first entanglement maximum significantly faster than P1 while maintaining robust performance across different spin dimensions.

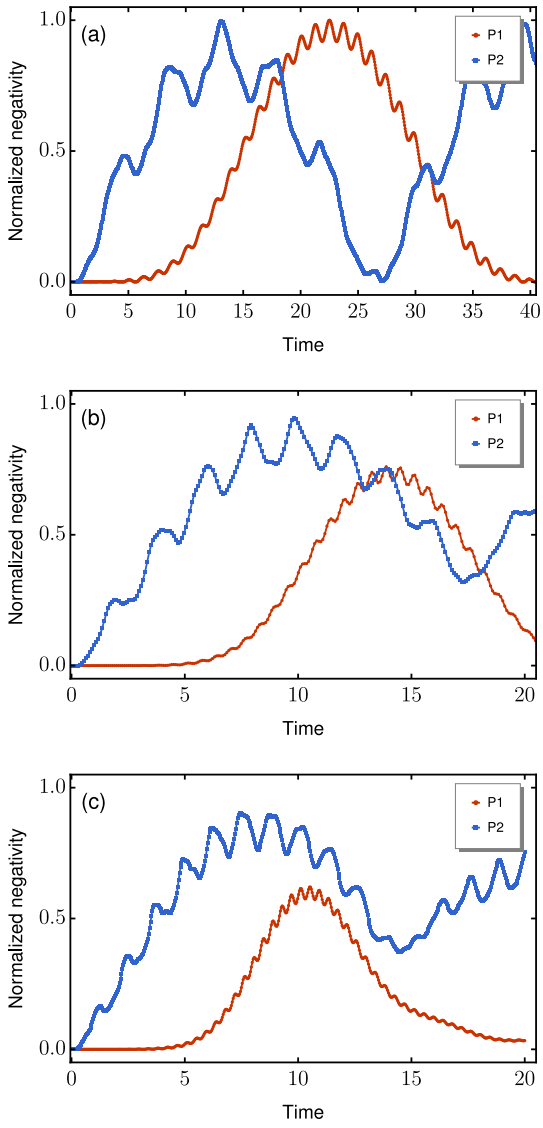

Fig. 2

Time evolution of the end-to-end negativity for (a) $s = 1/2$, (b) $s = 1$, and (c) $s = 3/2$. All traces correspond to the same dimerization ratio $\Delta/\delta = 10$. Results are shown for P1 (red curves) and P2 (blue curves).

In all cases, P2 exhibits faster entanglement generation and consistently achieves higher negativity values. In particular, for $s = 1/2$, both protocols output the Bell state $|\psi^+\rangle = (|01\rangle + |10\rangle)/\sqrt{2}$ when maximally entangled, though P2 requires a local $-\pi/2$ rotation to be applied on the z-axis of the qubit at site N, via application of the R_z gate. The fidelity dynamics concerning the target state $|\psi^+\rangle$ is shown in Fig. 3, where the necessary rotation for P2 has already been applied before the fidelity calculation.

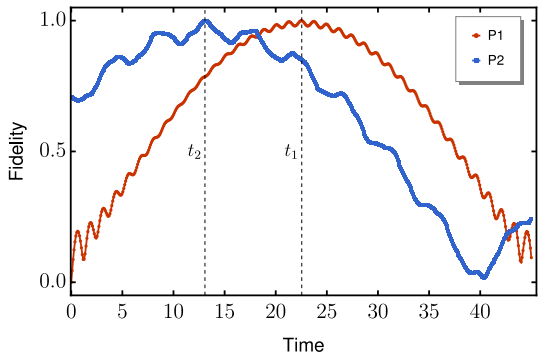

Fig. 3

TIME EVOLUTION OF FIDELITY WHEN CONSIDERING $|\psi^+\rangle$ AS THE TARGET STATE. THE RED LINE REPRESENTS P1, WHILE THE BLUE LINE REPRESENTS P2. THE TIME AT WHICH MAXIMAL ENTANGLEMENT IS ACHIEVED FOR EACH PROTOCOL IS MARKED WITH A DASHED VERTICAL LINE.

To determine the optimal value of B, we numerically analyze the relationship between B and the resulting negativity, identifying the parameter regimes and time scales that maximize negativity.

B. Robustness of the spin-1/2 protocol

The performance advantage of P2 is most relevant when it survives realistic imperfections. Therefore, we investigate its stability against static disorder, focusing on the spin-$1/2$ chain as a representative and experimentally accessible platform. To achieve this, we quantitatively assess its stability by introducing static disorder in spin-$1/2$ chains—a platform chosen for both its theoretical tractability and its experimental relevance. The analysis focuses on two fundamental channels of disorder that reflect distinct physical origins.

First, *on-site (diagonal) disorder* tests P2's sensitivity to variations in the fine-tuned boundary magnetic fields essential for its operation. To model fabrication-induced energy offsets, we introduce random local fields $h_i = Ed_i\delta$ with $d_i \in [-0.5, 0.5]$ uniformly distributed, where E scales the disorder strength relative to weak coupling δ. This modifies the Hamiltonian as:

$$H \to H + E\delta(d_1 S_1^z + d_{N-1} S_{N-1}^z). \tag{7}$$

For comparison, we apply identical perturbations to P1, establishing a performance baseline under equivalent conditions.

Second, *coupling (off-diagonal) disorder* captures imperfections in exchange interactions arising from material defects or control errors. The modified couplings $J_i \to J_i + Ed_i\delta$ yield the adjusted Hamiltonian:

$$H \to \sum_{i=1}^{N-1} (J_i + Ed_i\delta)\left(S_i^x S_{i+1}^x + S_i^y S_{i+1}^y\right). \tag{8}$$

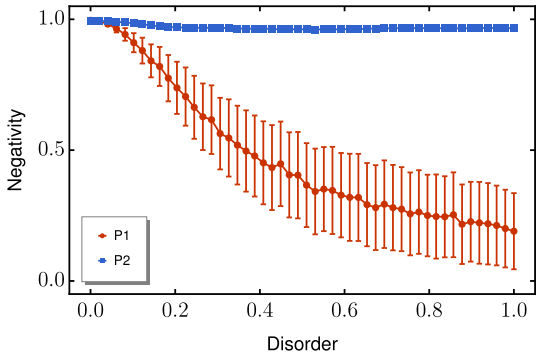

Fig. 4

AVERAGE PEAK NEGATIVITY AS A FUNCTION OF DIAGONAL DISORDER STRENGTH E. A RED LINE REPRESENTS P1, WHILE P2 IS SHOWN AS A BLUE LINE. THE RED AND BLUE BARS INDICATE THE STANDARD DEVIATION FROM THE MEAN FOR EACH PROTOCOL.

We investigated three distinct regimes: (i) pure on-site disorder, (ii) pure coupling disorder, and (iii) simultaneous disorder. For each disorder strength E, we ensure statistical reliability by computing the end-to-end peak negativity across 10^3 realizations..

Three cases were analyzed: (i) pure on-site disorder, (ii) pure coupling disorder, and (iii) both disorders acting simultaneously. We begin by analyzing pure on-site disorder. Figure 4 shows that P2 maintains excellent performance even at high disorder strengths, while P1 suffers significant entanglement degradation. This robustness is particularly valuable for practical implementations, as it allows for high entanglement generation (high negativity values) despite imperfections in the applied boundary magnetic fields.

A similar advantage emerges for coupling disorder (Fig. 5), where P2 maintains substantial entanglement ($\mathcal{N} \approx 0.8$) even at values of $E \approx 0.75\delta$. Interestingly, when diagonal and off-diagonal disorders are present simultaneously, P2 continues to outperform P1, as shown in Fig. 6. This consistent superiority across all disorder regimes confirms P2's exceptional resilience to typical solid-state fabrication imperfections.

C. Resistance to dephasing

A ubiquitous source of decoherence in solid-state devices is pure dephasing of the qubits that terminate the spin chain and interface it with external control circuitry. To assess its influence, we numerically evolve the *full* Lindblad master equation [see Eq. (2)], in which the term $\gamma \sum_{i=1}^{N}\Big(S_i^z \hat{\rho} S_i^z - \frac{1}{2}\{(S_i^z)^2, \hat{\rho}\}\Big)$ already models local dephasing for every site.

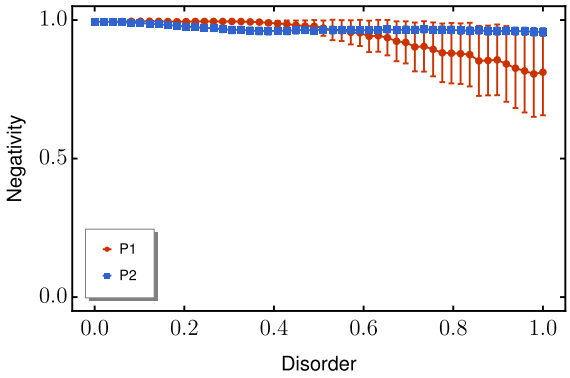

Fig. 5

AVERAGE PEAK NEGATIVITY AS A FUNCTION OF OFF-DIAGONAL DISORDER STRENGTH E. A RED LINE REPRESENTS P1, WHILE P2 IS SHOWN AS A BLUE LINE. THE RED AND BLUE BARS INDICATE THE STANDARD DEVIATION FROM THE MEAN FOR EACH PROTOCOL.

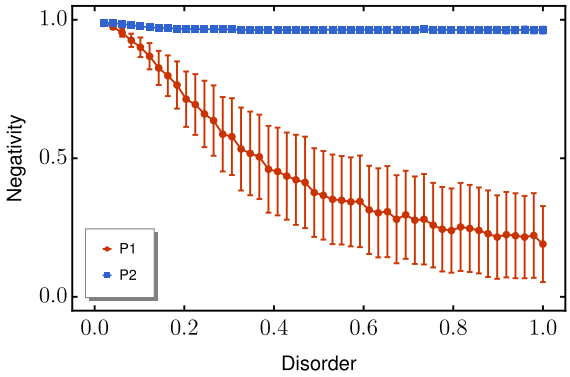

Fig. 6

AVERAGE PEAK NEGATIVITY AS A FUNCTION OF COMBINED DIAGONAL AND OFF-DIAGONAL DISORDER STRENGTH E. THE RED LINE REPRESENTS P1, WHILE P2 IS SHOWN AS A BLUE LINE. THE RED AND BLUE BARS INDICATE THE STANDARD DEVIATION FROM THE MEAN FOR EACH PROTOCOL.

By sweeping the dephasing rate γ and recording the peak end-to-end negativity, we obtain the curves in Fig. 7. The qualitative difference in decay trends between protocols P1 and P2 can be understood through the lens of the effective Hamiltonian [25] derived in the appendix.

IV. CONCLUSIONS

We have conducted a comprehensive numerical study of two entanglement generation protocols in XX spin chains, evaluating their performance across spin magnitudes $s = 1/2$, 1, and $3/2$, which reveals that the dual-port architecture (P2) consistently achieves higher entanglement on shorter timescales than its staggered counterpart (P1) for all the spin values considered. In addition to its speed advantage, P2 demonstrates strong robustness against both diagonal and off-diagonal disorder, as well as local dephasing noise, a resilience

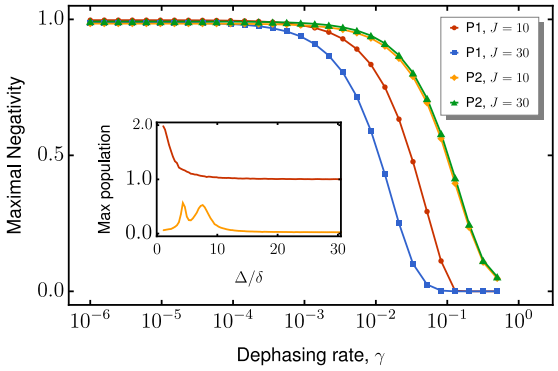

Fig. 7

PEAK END-TO-END NEGATIVITY UNDER BOUNDARY DEPHASING γ FOR COUPLINGS $\Delta = 10$ AND $\Delta = 30$ ($\delta = 1$). P2 OUTPERFORMS P1, SHOWING GREATER ROBUSTNESS WITH SLOWER ENTANGLEMENT DECAY. THE INSET REVEALS P2 ALSO MAINTAINS SIGNIFICANTLY LOWER BULK EXCITATION ACROSS BOTH REGIMES.

attributed to its design, which minimizes excitation of the bulk spins through optimized boundary control and coupling symmetry, thereby enhancing coherence and reducing vulnerability to noise. These features make P2 not only more efficient but also more scalable and robust, establishing it as a strong candidate for practical implementations in entanglement-based quantum information processing, and future work may explore the extension of this protocol to larger spin networks and its embedding within hybrid quantum architectures [26], directions which could be further enriched by integrating advanced techniques such as color-engineered communication channels [27], star-like entanglement hubs for multi-qubit interfacing [28], and dissipative stabilization mechanisms for steady-state entanglement [29].

ACKNOWLEDGMENTS

This work was partially supported by Coordenação de Aperfeiçoamento de Pessoal de Nível Superior (CAPES, Finance Code 001), Conselho Nacional de Desenvolvimento Científico e Tecnológico (CNPq), and Instituto Nacional de Ciência e Tecnologia de Informação Quântica (INCT-IQ).

APPENDIX

We consider an N-site spin-$1/2$ XX chain with alternating couplings, described by

$$H = \sum_{i=1}^{N-1} J_i \left(S_i^x S_{i+1}^x + S_i^y S_{i+1}^y \right) + \sum_{i=1}^{N} B_i S_i^z, \qquad (9)$$

where $J_i = \Delta$ (strong) or δ (weak), and $B_i = \omega/2$ is a uniform magnetic field. We consider emitter (e) and receiver (r) qubits coupled at the boundaries via

$$H_{\text{er}} = \frac{\omega}{2}(S_e^z + S_r^z) + \lambda \left(S_e^+ S_1^- + S_r^+ S_N^- + \text{H.c.} \right), \qquad (10)$$

leading to the full Hamiltonian $H_S = H + H_{\text{er}}$, with all $J_i = \Delta$ and $\lambda = \delta$ for P2.

Applying the Jordan-Wigner transformation maps the spin system to noninteracting fermions. The resulting Hamiltonian in the single-excitation subspace becomes

$$H'_S = \sum_{k=1}^{N} E_k f_k^\dagger f_k + \sum_{k=1}^{N} \overline{\lambda}_k \left(c_e^\dagger f_k + (-1)^{k-1} c_r^\dagger f_k + \text{H.c.} \right), \tag{11}$$

where

$$E_k = \Omega + 2\Delta \cos\left(\frac{k\pi}{N+1}\right), \tag{12}$$

$$\overline{\lambda}_k = \lambda \sqrt{\frac{2}{N+1}} \sin\left(\frac{k\pi}{N+1}\right), \tag{13}$$

.

Transforming to the interaction picture concerning $H_0 = \sum_k E_k f_k^\dagger f_k + \frac{\omega}{2}(S_e^z + S_r^z)$ gives

$$\bar{H}_S(t) = \sum_k \overline{\lambda}_k \left[\left(c_e^\dagger f_k + (-1)^{k-1} c_r^\dagger f_k \right) e^{i\zeta_k t} + \text{H.c.} \right], \tag{14}$$

with detuning $\zeta_k = \omega - E_k$.

In the dispersive regime $\overline{\lambda}_k/\zeta_k \ll 1$, second-order perturbation theory yields an effective Hamiltonian that directly couples the boundary qubits via virtual excitations:

$$H_{\text{eff}} = \chi \left(c_e^\dagger c_r + c_e c_r^\dagger \right), \tag{15}$$

with

$$\chi = \sum_k \frac{\overline{\lambda}_k^2}{\zeta_k}. \tag{16}$$

This mediated interaction allows coherent entanglement generation without significant excitation of the channel. The average number of excitations in the chain during evolution up to the entanglement generation time $\tau = \pi/4\chi$ is

$$\langle n \rangle = \sum_k \int_0^\tau \frac{\left\langle f_k^\dagger(t) f_k(t) \right\rangle}{\tau} dt \approx N \left(\frac{\pi\delta}{2\Delta}\right)^2. \tag{17}$$

Thus, the excitation leakage remains negligible as long as $\sqrt{N}\delta/\Delta \ll 1$.

Moreover, the third-order corrections scale as $N\overline{\lambda}_k^3/\zeta_k^2$, so the validity of the effective model requires

$$N \ll \frac{\zeta_k}{\overline{\lambda}_k}. \tag{18}$$

REFERENCES

[1] A. Acín, I. Bloch, H. Buhrman, T. Calarco, C. Eichler, J. Eisert, D. Esteve, N. Gisin, S. J. Glaser, F. Jelezko, S. Kuhr, M. Lewenstein, M. F. Riedel, P. O. Schmidt, R. Thew, A. Wallraff, I. Walmsley, and F. K. Wilhelm, "The quantum technologies roadmap: a european community view," *New J. Phys.*, vol. 20, p. 080201, 2018.

[2] E. Chitambar and G. Gour, "Quantum resource theories," *Rev. Mod. Phys.*, vol. 91, p. 025001, 2019.

[3] S. Takeda, T. Mizuta, M. Fuwa, P. van Loock, and A. Furusawa, "Deterministic quantum teleportation of photonic quantum bits by a hybrid technique," *Nature*, vol. 500, pp. 315–318, 2013.

[4] C. L. Degen, F. Reinhard, and P. Cappellaro, "Quantum sensing," *Rev. Mod. Phys.*, vol. 89, p. 035002, 2017.

[5] C. H. Bennett and G. Brassard, "Quantum cryptography: Public key distribution and coin tossing," *Theor. Comput. Sci.*, vol. 560, pp. 7–11, 2014.

[6] A. Einstein, B. Podolsky, and N. Rosen, "Can quantum-mechanical description of physical reality be considered complete?," *Phys. Rev.*, vol. 47, pp. 777–780, 1935.

[7] A. Furusawa, J. L. Sørensen, S. L. Braunstein, C. A. Fuchs, H. J. Kimble, and E. S. Polzik, "Unconditional quantum teleportation," *Science*, vol. 282, pp. 706–709, 1998.

[8] S. Bose, "Quantum communication through spin chain dynamics: an introductory overview," *Contemp. Phys.*, vol. 48, pp. 13–30, 2007.

[9] M. P. Estarellas, I. D'Amico, and T. P. Spiller, "Robust quantum entanglement generation and generation-plus-storage protocols with spin chains," *Phys. Rev. A*, vol. 95, p. 042335, 2017.

[10] G. Neto, M. de Ponte, and M. H. Y. Moussa, "Nonlocal dissipative tunneling for high-fidelity quantum-state transfer between distant parties," *Phys. Rev. A*, vol. 85, p. 052303, 2012.

[11] R. Blatt and C. F. Roos, "Quantum simulations with trapped ions," *Nat. Phys.*, vol. 8, pp. 277–284, 2012.

[12] P. Krantz, M. Kjaergaard, F. Yan, T. P. Orlando, S. Gustavsson, and W. D. Oliver, "A quantum engineer's guide to superconducting qubits," *Appl. Phys. Rev.*, vol. 6, p. 021318, 2019.

[13] M. W. Doherty, N. B. Manson, P. Delaney, F. Jelezko, J. Wrachtrup, and L. C. L. Hollenberg, "The nitrogen-vacancy colour centre in diamond," *Phys. Rep.*, vol. 528, pp. 1–45, 2013.

[14] R. Hanson, L. P. Kouwenhoven, J. R. Petta, S. Tarucha, and L. M. K. Vandersypen, "Spins in few-electron quantum dots," *Rev. Mod. Phys.*, vol. 79, pp. 1217–1265, 2007.

[15] X. Wang, A. Bayat, S. G. Schirmer, and S. Bose, "Robust entanglement in antiferromagnetic heisenberg chains by single-spin optimal control," *Phys. Rev. A*, vol. 81, p. 032312, Mar 2010.

[16] J. M. Martinis, S. Nam, J. Aumentado, and C. Urbina, "Rabi oscillations in a large josephson-junction qubit," *Phys. Rev. Lett.*, vol. 89, p. 117901, 2002.

[17] J. A. Schreier, A. A. Houck, J. Koch, D. I. Schuster, B. R. Johnson, J. M. Chow, J. M. Gambetta, J. Majer, L. Frunzio, M. H. Devoret, S. M. Girvin, and R. J. Schoelkopf, "Suppressing charge noise decoherence in superconducting charge qubits," *Phys. Rev. B*, vol. 77, p. 180502, 2008.

[18] I. Bloch, J. Dalibard, and W. Zwerger, "Many-body physics with ultracold gases," *Rev. Mod. Phys.*, vol. 80, pp. 885–964, 2008.

[19] G. Vidal and R. F. Werner, "Computable measure of entanglement," *Phys. Rev. A*, vol. 65, p. 032314, 2002.

[20] L. C. Venuti, S. M. Giampaolo, F. Illuminati, and P. Zanardi, "Long-distance entanglement in spin systems," *Physical Review Letters*, vol. 96, no. 24, p. 247206, 2006.

[21] F. Verstraete, M. M. Wolf, and J. Ignacio Cirac, "Quantum computation and quantum-state engineering driven by dissipation," *Nature Physics*, vol. 5, pp. 633–636, 2009.

[22] J. Dias, C. W. Wächtler, K. Nemoto, and W. J. Munro, "Entanglement generation between distant spins via quasilocal reservoir engineering," *Physical Review Research*, vol. 5, no. 4, p. 043295, 2023.

[23] P. Kurpiers, P. Magnard, T. Walter, and et al., "Heralded entanglement between solid-state qubits separated by a meter," *Nature*, vol. 558, no. 7709, pp. 264–267, 2018.

[24] Y. Bahri, R. Vosk, E. Altman, and A. Vishwanath, "Localization and topology protected quantum coherence at the edge of 'hot' matter," *Nature Communications*, vol. 6, p. 7341, 2015.

[25] E. K. Soares, G. D. de Moraes Neto, and F. M. Andrade, "Comparative analysis of robust entanglement generation in engineered xx spin chains," *Entropy*, vol. 27, no. 7, p. 764, 2025.

[26] P. Forn-Díaz, L. Lamata, E. Rico, J. Kono, and E. Solano, "Ultrastrong coupling regimes of light-matter interaction," *Rev. Mod. Phys.*, vol. 91, p. 025005, 2019.

[27] G. de Moraes Neto, M. de Ponte, and M. H. Y. Moussa, "Colored channels for high-fidelity information transfer and processing between remote multi-branch quantum circuits," *Europhys. Lett.*, vol. 103, p. 43001, 2013.

[28] R. Grimaudo, A. S. Magalhães de Castro, A. Messina, and D. Valenti, "Spin-chain-star systems: Entangling multiple chains of spin qubits," *Fortschr. Phys.*, vol. 70, p. 2200042, 2022.

[29] G. de Moraes Neto, V. Teizen, V. Montenegro, and E. Vernek, "Steady many-body entanglements in dissipative systems," *Phys. Rev. A*, vol. 96, p. 062313, 2017.